Development of a New NDT Method Using Thermography for Composite Inspection on Aircraft with Portable Military Thermal Imager

Pierre SERVAIS, Belgian Air Force NDT squadron commander,
Compentence Center Flying Material, Brussel, Belgium

Abstract. TNDT (Thermal Non Destructive Testing) is now an emerging method that comes out of laboratory since a few years. It is here proposed to investigate, compare and quantify the different possibilities to use thermography in stead of radiography or ultrasonic testing on composite parts in maintenance of aircrafts. The new idea is to use military thermal imagers because the detector is now a very sensitive infrared focal plane array.

1. Introduction

Thermography is particularly adapted for non destructive testing on composite providing to the inspector a global mapping of the part where ultrasonic testing will give only a local result in maintenance (working here with classical portable UT equipment). TNDT can be used on different materials

- Monolithic composite in CFRP (Carbon Fibre Reinforced Plastic)
- thin metal skin on honeycomb structure (like aircraft doors)
- epoxy resin with glass fibre reinforcement plastic or GFRP
- panel skins with CFRP like helicopter blades

Thermal imagers used for night surveillance by the infantry (see figure 1) are very robust, portable and even waterproof. They can now show very faint differences of temperature (less than 0.07 K) and so can be a very good instrument for NDT when using a .

Figure 1 : military Thermal imager used by Belgian Defense

This thermal control contributes to highlight the most prominent types of discontinuities detected in aerospace composites including [1]

- water ingress or moisture which can degrade the mechanical properties of some resins or lead to freeze inside the part causing ice expansion forces during the flight (see picture 2 for honeycomb composite part with view of hotter area at the centre of the piece shown in white)
- disbond or delamination resulting from low strength in the resin
- impact damage on the taxiway (FOD – Foreign Object Damage) or caused by bird strike or by a dropped tool during maintenance
- Metallic or non metallic inclusions which can reduce strength by kinking the fibres around the inserted material

Some defects like water ingress cause high thermal difference on the surface as seen on figure 2 below.
This thermal difference depends on their characteristics (mainly thermal resistance), their dimensions and their depth in the part. So the camera should have good thermal resolution (NETD or Noise Equivalent Temperature Difference). [2] Recent work made by Italian Air Force showed that 0.1 ml water ingress in one cell of honeycomb flap of AMX aircraft could show a thermal difference of 1°C when surface is heated with a flow of 15000 W/m^2.[3] The figure below is an example of thermal signature of water ingress:

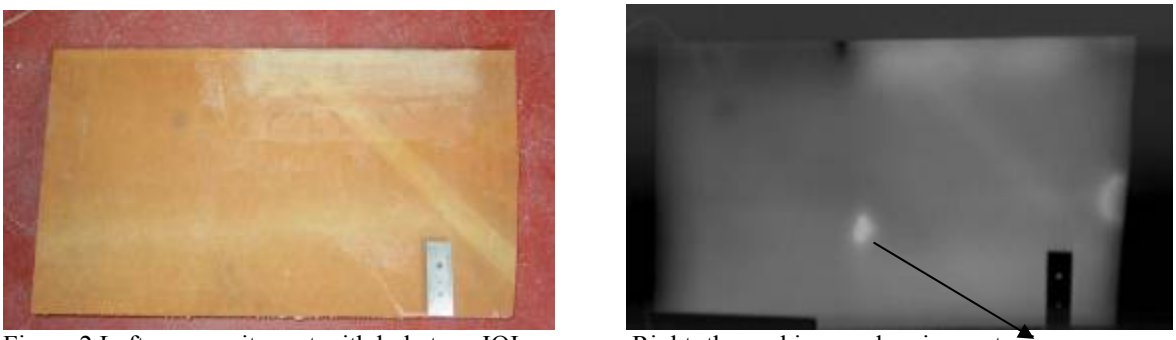

Figure 2 Left: composite part with hole type IQI Right: thermal image showing water ingress

2. Application to F-16 leading edge flaps and Agusta rotor blades

The inspection of composite materials is an increasingly important topic due to the expanding number of uses to which such materials are being put. Due to its lightness, composite is used in large quantities in aeronautical applications. For example, Belgian F-16 leading edge flaps and Agusta rotor blades are exclusively built in composite.

Composite materials can be affected by manufacturing processes defects (voids due to volatile resin components, foreign bodies, ply cracking, delaminations, bonding defects...) and by in-service defects (fracture of fibres, cracks, delaminations, ingress of moisture, inclusions, impact damage,...).

In case of F-16 leading edge flaps and Agusta rotor blades, it is challenge of outstanding importance to detect defects as precisely as possible. This should avoid unnecessary scraping of expensive material and increase serviceability of parts.

Until now, only tap testing is used to verify integrity of these composite parts, mainly because radiography can not detect delamination and because ultrasonic testing (UT) is a point to point technique not really appropriate for parts as long as blades with a length of 5

meters. Another problem for UT will come for the control of honeycomb structure because of the presence of air which does not transmit the ultrasound pulse easily.

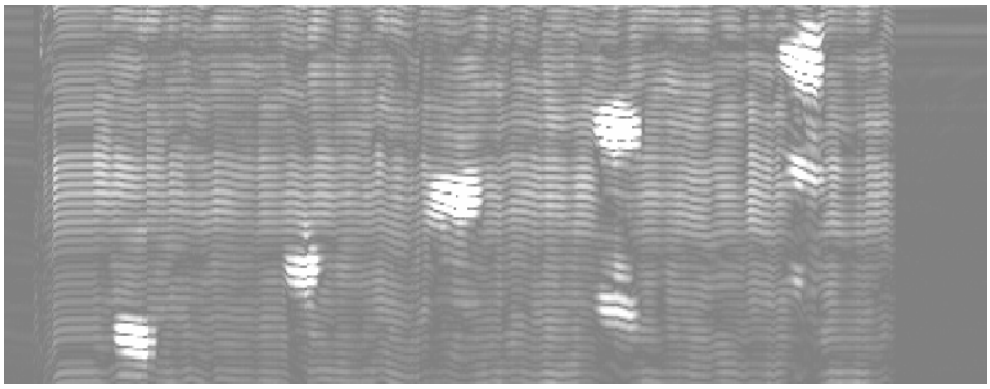

Figure 2b: Ultrasonic B-scan view of composite plate showing 5 flat bottom holes

Tap test delivers only approximate information on the wellbeing of the material and we need to quantify the defect for correct evaluation in accordance with given rejection criteria.

It is thus important to develop a more reliable non destructive testing methodology especially adapted to composite materials knowing the acceptance criteria used in maintenance.

Thermography is an incoming non destructive testing tool that presents some key advantages in comparison with the available technologies, namely:

- It is totally non-contacting and non-invasive.
- It can inspect relatively large areas in a single snapshot.
- The data are pictorial format resulting in rapid decisions.
- The data are easily stored and retrieved with any classical laptop.
- The current price of IR camera is now competitive with other NDT method.
- It allows fast inspection rates (on line information).
- The security of personnel is guaranteed when compared to radiography.

Furthermore for air forces, there is no real difficulty to obtain adequate equipments (IR camera, thermal stimulation units, frame grabbers and laptop) because these are widely used in the Defence. This should reduce drastically the cost of the application and facilitate a large diffusion of this NDT technology amongst all Defence organizations. A real case example is shown in figure 3 with a flying composite part coming from our Alphajet (used as training aircraft with French Air Force in Cazaux).

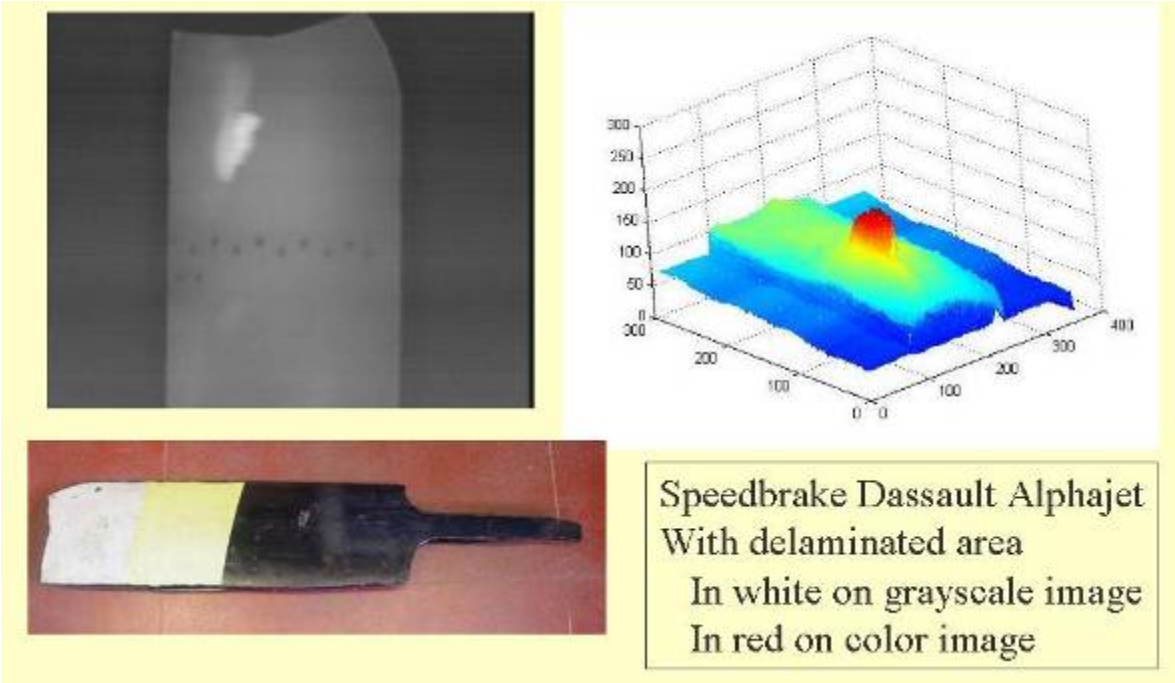

Figure 3: Example of use of military thermal imager to detect delaminations on our training aircraft

3. Choice of heating procedures

3.1 Experimental test of different heaters

A first approach will compare the most popular heaters like:

- optical heating (flash tubes, projector, tubular halogen lamps, UV light) ,
- air flux heating (air dryer and thermal paint remover)
- IR heater like portable electrical heater 2700 W
- specific heating blankets used also for composite repair in maintenance

The comparison will take into account main heating properties: repeatability, uniformity, timeliness, duration. The thermal imager can easily be used to retrieve these characteristics but a real laboratory camera (like FLIR SC3000) can also be used to quantify temperatures directly and more easily.

Figure 4 : classical heaters used for thermal sollicitations

3.2 Study of obtained thermograms

A second approach will be an experimental study of raw images obtained using several heaters. For each heating method, the more adequate parameters to be used are determined in order to optimise defect detection in a raw image of a known sample:

- final temperature obtained
- duration of the heating (flash or long pulse)
- location and orientation of the heater, start up time to be at constant temperature

The best results are obtained with two sets of 6 halogen lamps used initially for drying the painted pieces at painting workshop. The set up permits us to produce 2x6x250 W, giving 3000 Watts thermal power with two directions with a very mobile configuration as shown in figure 5.

Figure 5 : Set up used for infrared testing of composite speedbrakes (front and rear view showing 2 x 6 halogen lamps used to generate the thermal pulse)

4. IR detectors

4.1 Characteristics of the thermal detector

A Theoretical comparison between the available detectors will take into account the different characteristics of the thermal detector:

We compare our military imager from Thalès with a classical laboratory IR camera FLIR SC3000

- Type of IR detector : our military thermal system uses a FPA (Focal Plane Array) HgCdTe hybridized on a silicon CMOS readout circuit
- Type of cooler (our photovoltaic detector is cooled by miniature Stirling-cycle rotary cooler)
- Noise equivalent temperature difference, here around 80 mK measured at the military air conditioned laboratory on a calibrated blackbody (with a precise regulation at 0.01°C). An example of an obtained thermogram is given in fig 6.

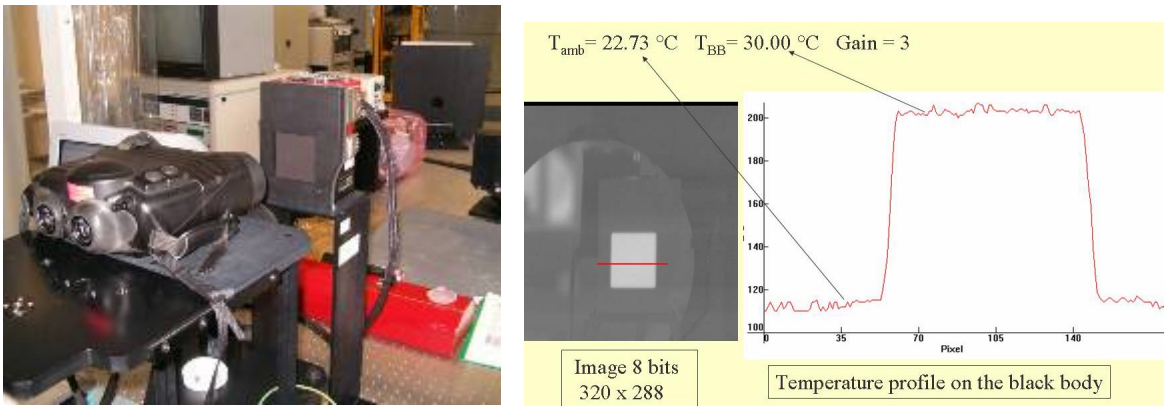

Figure 6: Thermal image made on our calibrated blackbody and temperature profile (graylevel units)

- Detectivity D* (sensitivity figure of merit of an infrared detector) > 2.3 10^{11} Jones for our camera.
- Minimum resolvable temperature difference (the smallest temperature difference that an operator can clearly distinguish out of the noise) checked with calibrated blackbody at the laboratory with different observers following ASTM E 1213 [4].
- slit response function (spatial resolution) also compared during other tests with hole type IQI placed on part (see figure 2 right) to have a reference spatial information at lower constant temperature than the part [5]
- Selection of the proper atmospheric band (longer wave 8-12 µm for our military thermal imager)

4.2 Study of obtained thermograms

An experimental comparison of raw images obtained by different detectors on the same test samples containing different types of defects, of different sizes and at different depths are used to choose the best set up for our thermal imager so that we can obtain equivalent results with FLIR SC3000.

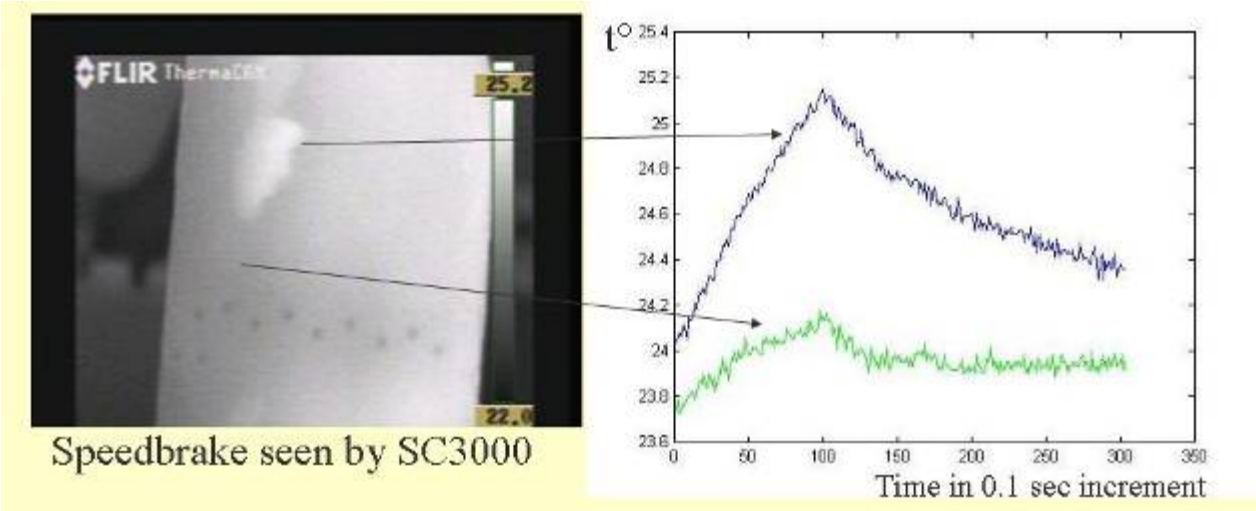

Figure 7: Alphajet speedbrake tested with FLIR SC3000 with T° evolution during 30 sec on 2 relevant points showing a temperature contrast of 1.2 ° C obtained after 10 sec heating duration between the delaminated area and the composite part (black points are rivets row located at the backside of the part, see figure 5 right for visible rear view of the piece)

5. Choice of a thermography technique

The main goal is to develop a portable inspection method, so it is first experienced with pulse thermography then pulse phased thermography and Lockin thermography. This inspection relies on a short thermal stimulation pulse, with duration of a few seconds for low conductivity specimens (such as graphite epoxy laminates). Such thermal stimulation allows direct deployment with convenient heating sources and prevents damage to the component. The pulse thermography consists of briefly heating the part to inspect and then recording the temperature decay curve (as shown in figure 7). The temperature of the piece changes rapidly after the initial thermal pulse because the thermal front propagates by diffusion, under the surface and also because of radiation and convection losses. The presence of defects reduces the diffusion rate so that when observing the surface temperature, defects appear as areas of different temperatures with respect to surrounding sound area once the thermal front has reached them. Consequently, deeper defects will be observed later and with a reduced contrast.

6. Signal processing :

After the choice of the technique and the calibrated sample, it is necessary to make signal processing of the thermal acquisition, mainly for the following points:

6.1 Noise considerations

- Experimental determination of noise from the IR detector, electronic noise, noise from external source, noise caused by object inhomogeneity coming mainly from the top coat painting. The measurements of NETD were made inside a white room (optronics laboratory) on a calibrated blackbody (regulated at 0.01°C) for 10000 points (100 x 100 window) with 40 different images.

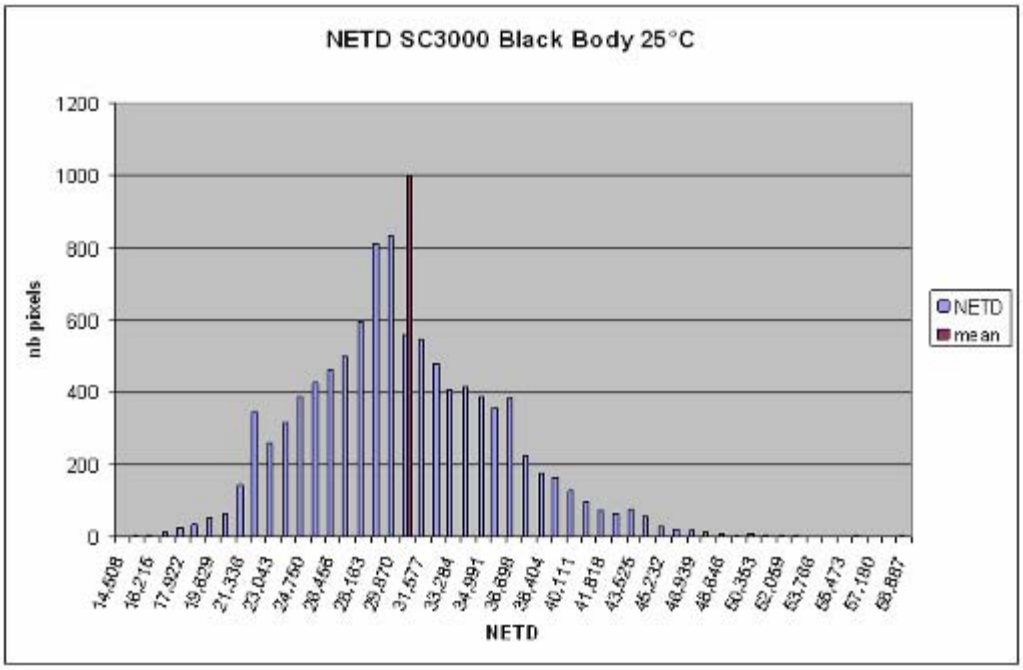

Figure 8: NETD in mK measured on a blackbody for FLIR SC3000 at laboratory

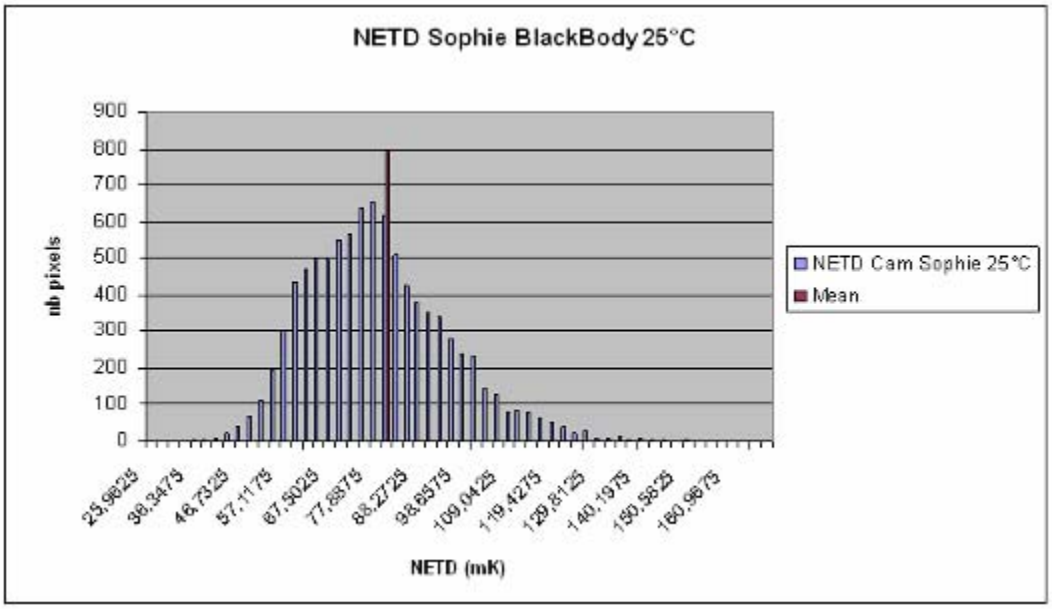

Figure 9: NETD in mK measured on a blackbody for military imager at laboratory

The above figures show a mean value of NETD for commercial IR camera at 30,6 mK and a higher expected value for our thermal imager at 78,92 mK. These values are 10 mK above the value found in the specifications of the manufacturer (20 mK for FLIR data and 70 mK for Thalès-Sofradir detector data).

We can also clearly notice an asymmetric distribution of NETD as noticed in the paper over "FPA as research tool" [7]

The noise can be easily reduced by adding lots of thermograms using an averaging procedure as shown in figure 8 for a composite calibre.

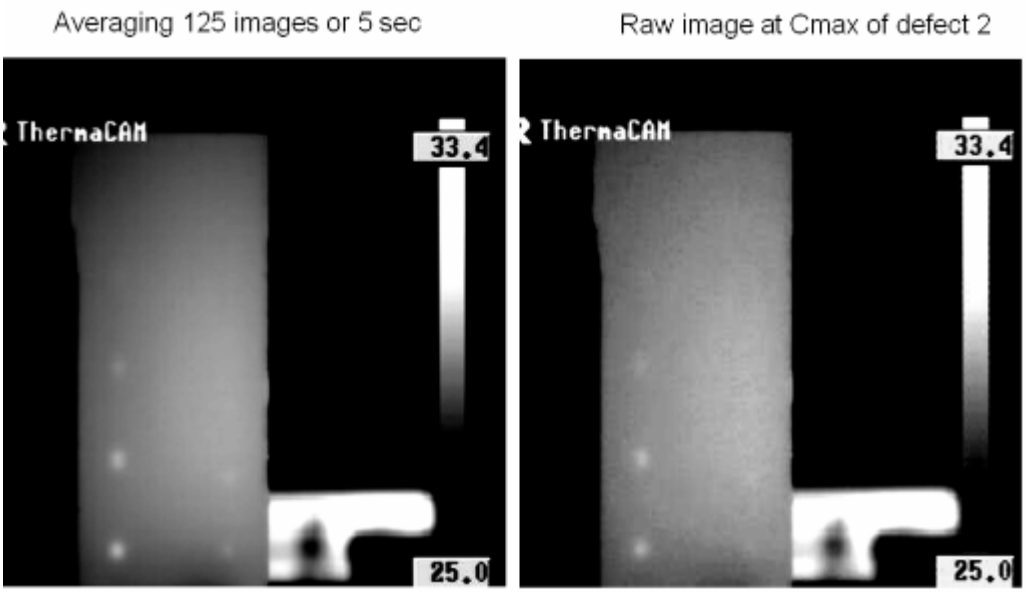

Figure 8, Left processed image, Right raw thermogram of a CFRP sample with defects.

By adding 125 images, we obtained a Signal to Noise Ratio 4 times higher for the 3 first defects detected.

If we apply the same analysis (averaging images) on blackbody images, we can also quantify the influence of the number of images accumulated versus NETD. The table 1 below summarizes the reduction of noise in function of number of images used in averaging process. A good compromise will be 4

Nb averaged images	NETD calculated
One raw image	30,5 mK
2 images	23,5 mK
4 images	15,95 mK
16 images	13,43 mK

Table 1 : influence of Nb of accumulated images on NETD for FLIR SC3000

6.2 Camera calibration

A first problem for the viewing comes from the optical noise. To correct the vignetting effect present in every optical instrument due to the presence of the aperture lens, the military camera uses an internal EPROM with the NUC coefficients (Non Uniformity Correction). This calibration is made yearly for each camera on the thermal imager bench at optronical laboratory. The real temperature computations to establish a correct calibration curve is also made on a blackbody inside a white room.

Then to increase the detectability on every IR image, a choice of the best contrast computation must be made: absolute contrast, running contrast, normalized contrast or differential absolute contrast provide a good detectability of known defects and permit segmentation of the defect using morphological operations as shown in figure 9.

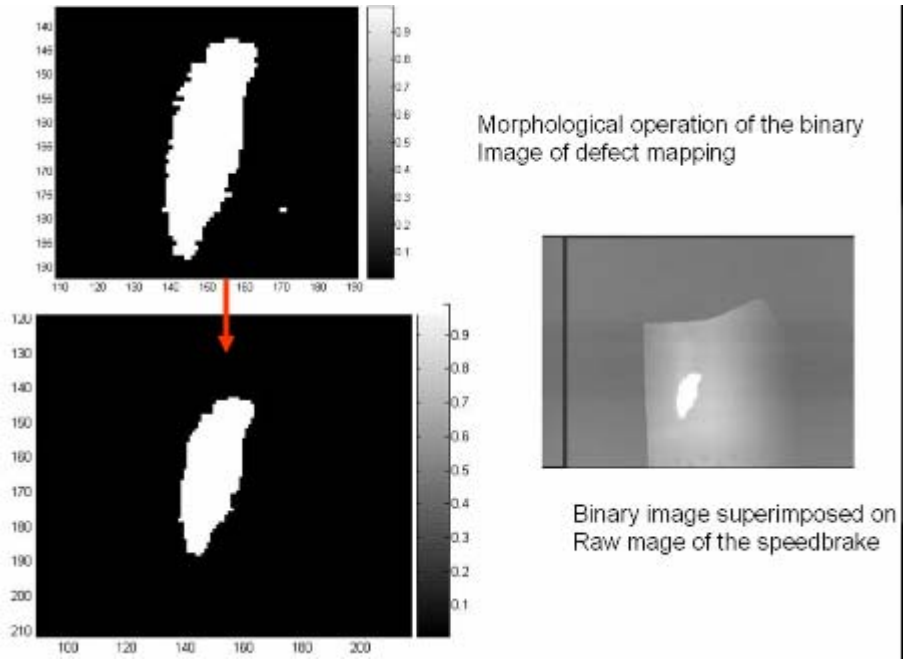

Figure 9 : Segmentation of a real delamination found in Belgian Alphajet speedbrake

The morphological process is here a closing operation: the image is first binarized using a threshold then eroded and dilated to obtain a good segmentation of the delamination which permits us to make a correct sizing of the area of the defect. The final step is to evaluate the delamination in accordance with rejection criteria defined by the manufacturer.

7. Experimental results on known samples

After having processed the acquisition, some important features must be evaluated like:

(1) Reduction in image contrast with defect depth (see figure 8 for three first flat bottom holes seen bottom left of the composite sample)

(2) Effect of host material thermal properties like water ingress (see figure 2 right) or rivets row giving a negative thermal contrast (so appearing darker on thermograms, see figure 3 and 7)

(3) Temperature decay at the surface over defect for different depths (see fig 11)

(4) Thermal contrast produced at the surface by defects at different depths.

(5) Thermal signature of different defects: water ingress, delamination and flat bottom holes (see respectively figure 2, figure 3 and figure 8).

The following sample will be used as homemade calibre and will permit to study the different parameters of the technique:
A monolithic composite panel made of 84 plies of CFRP with two rows of flat bottom holes (FBH) with two different diameters 10 mm and 5 mm at different depths (see table 2)

row of 5 mm diameter	Row of 10 mm diameter
Defect 1 : 0.91 mm	Defect 1 : 0.81 mm
Defect 2 : 1.51 mm	Defect 2 : 1.31 mm
Defect 3 : 2.11 mm	Defect 3 : 1.91 mm
Defect 4 : 2.36 mm	Defect 4 : 2.51 mm
Defect 5 : 2.61 mm	Defect 5 : 3.01 mm
Defect 6 : 3.01 mm	

Table 2 : distance from heated surface for each FBH of the sample

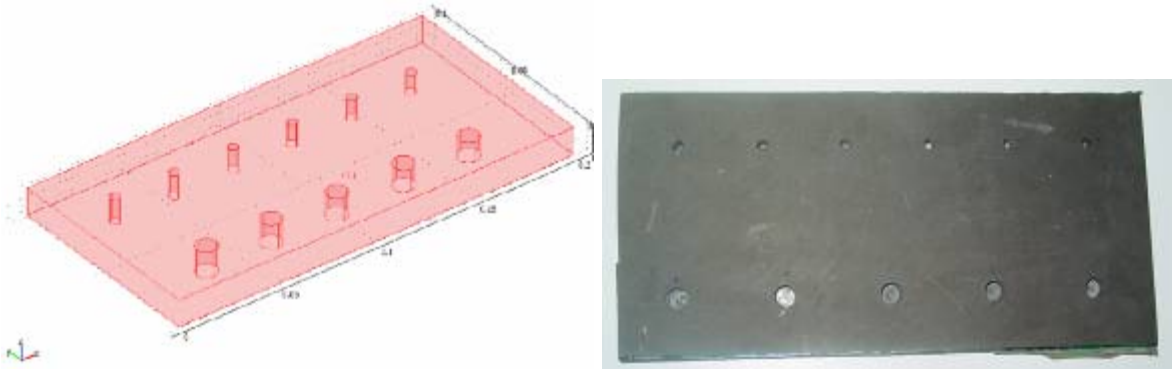

Figure 10 : Composite calibre Left : model; Right : rear side view of the part with FBH

This sample was first heated during 30 seconds with the two sets of halogen lamps shown in figure 5. We can now represent the temperature evolution (the unit is here graylevel which correspond to a known temperature difference) for one defect. The upper curve represents the temperature surface above defect 4 which is higher than the temperature of composite part. It is easier to represent the temperature contrast multiplied by 10 to clearly see the time evolution and the best visibility period (here between 15 till 50 seconds).

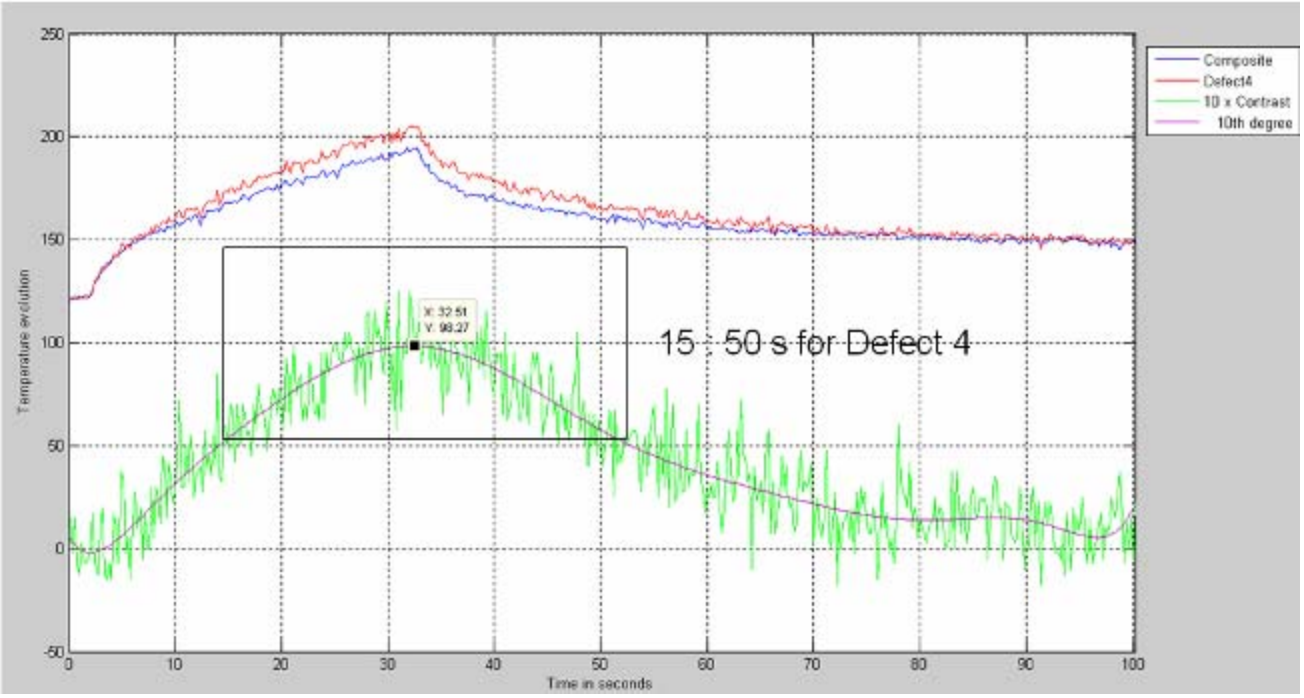

Figure 11 : Temperature evolution over 100 s for defect4 with temperature contrast (x10)

For a correct set up (heating duration 30 s with 3000 W located at 50 cm of the part), we can easily determine the time of the maximum contrast in function of the depth of the defect by use of a polynomial fitting (here with 10 coefficients). We can also analyse the amplitude of the maximum temperature contrast in function of the depth and the diameter of the defect. For this CFRP (typical composite fibre used on Airbus aircraft), we can see all the defects of 10 mm diameter but for 5 mm diameter, we come to a limit due to the spatial resolution of our set up but the typical rejection criteria in maintenance will be an half inch size delamination, so we will focus on the defects of 10 mm diameter. By testing the different parameters on a known calibre, we determined the best parameters for the acquisition and signal processing of the pulse thermography sequence (see table 3).

Parameter	**Numerical value**
Frames per sec	25 fps
Acquisition time	100 seconds
Number of raw images	2500
Size of each image	352 x 288 lines
Image type storage	RGB (24 bits)
Size of each image	352 x 288 lines
Video compression	None
ADC	12 bits
Duration of heat pulse	30 seconds
Time averaging	5 images => 5 Hz signal
Polynomial fitting	10 coefficients
Storage size	18 Mb

Table 3 : parameters used for the thermal acquisition and signal processing

Another important signal processing to apply on all obtained images is a spatial filtering to increase the seeability and reduce the noise content of each image (see figure 12)

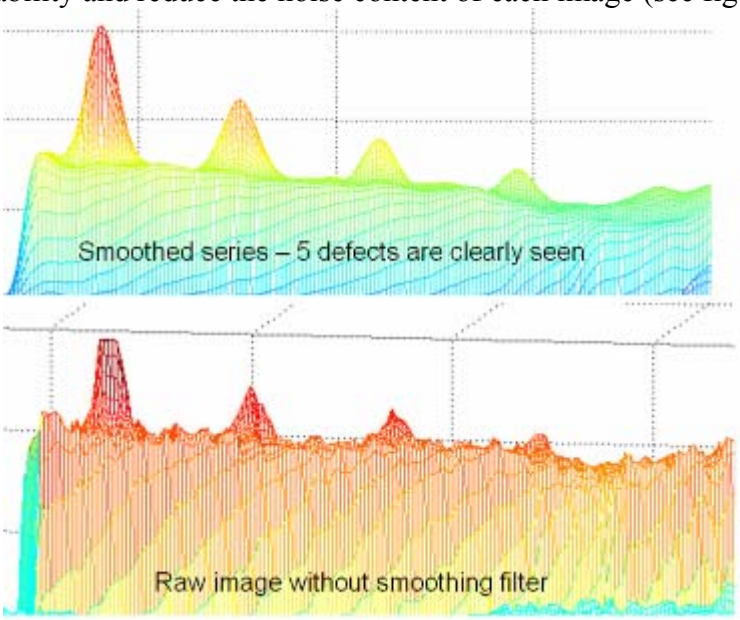

Figure 12: influence of smoothing filtering on temperature profile line across the 5 defects

By studying the 5 defects of 10 mm diameter at different depth, we can conclude that with our setup, we can detect till 3 mm depth inside CFRP panel. If we try deeper defects, we certainly come to a problem of contrast maximum which will stay undetected due to noise level of any thermogram (even if we increase the time averaging and the smoothing operations). If we represent the contrast temperature evolution of each defect like it was done for defect 4 in figure 11, we come to the following numerical values for test :

10 mm Defect Nb	Time of contrast Max	Amplitude of contrast Max
1	24 sec	51 ADU
2	27,5 sec	23 ADU
3	30,5 sec	16 ADU
4	32,5 sec	10 ADU
5	38 sec	5 ADU

Table 4 : results of study for each defect (FBH) of temperature contrast evolution in CFRP panel

By looking to theses values, we clearly see that deeper the defect, longer becomes the time of maximum contrast and lower is the amplitude of this contrast. In fact the observation time is a function (in a first approximation) of the square of depth (Cielo et al., 1987) and the loss of constrast is inversely proportional to the cube of the depth (see figure 13 for experimental results). The inverse problem of finding the depth Z of a defect in function of the time of maximum contrast and in function of the amplitude of maximum contrast Cmax was originally proposed by Balageas et al. in 1987 with an equation like:

$$z_{defect} = 0.6722\sqrt{time_{C_{\max}}}\,(C_{\max})^{-0.258}$$

But for our setup here, it is not really possible to get good results (with a good reliability) to find the depth of our defects so we must use another technique like working with phase thermography.

By taking 5 ADU (graylevel out of 256 different values) as limiting factor for the detectability regarding also our NETD, we can decide that 3 mm will be the deepest defect seen with this setup (30 seconds heating pulse, 3000 W at 50 cm distance from entry surface of composite panel, time averaging on 5 images). By plotting the amplitude of maximum contrast in function of depth, we can easily see the non linear evolution of the contrast, giving a very good detectability till 2 mm but going quickly till very low contrast when coming to 3 mm of depth under heated surface of the part. This is also in agreement with the following empirical rule of thumb: "the radius of the smallest detectable defect should be at least one to two times larger than its depth under the surface" (Vavilov and Taylor, 1982). For a depth of 3 mm, the radius must be at least 3 to 6 mm or a diameter of 6 to 12 mm. For a depth of 2 mm, we can see all defects of 10 mm diameter and the first 3 of 5 mm diameter which is also in accordance with the empirical rule of thumb, even for a military thermal imager.

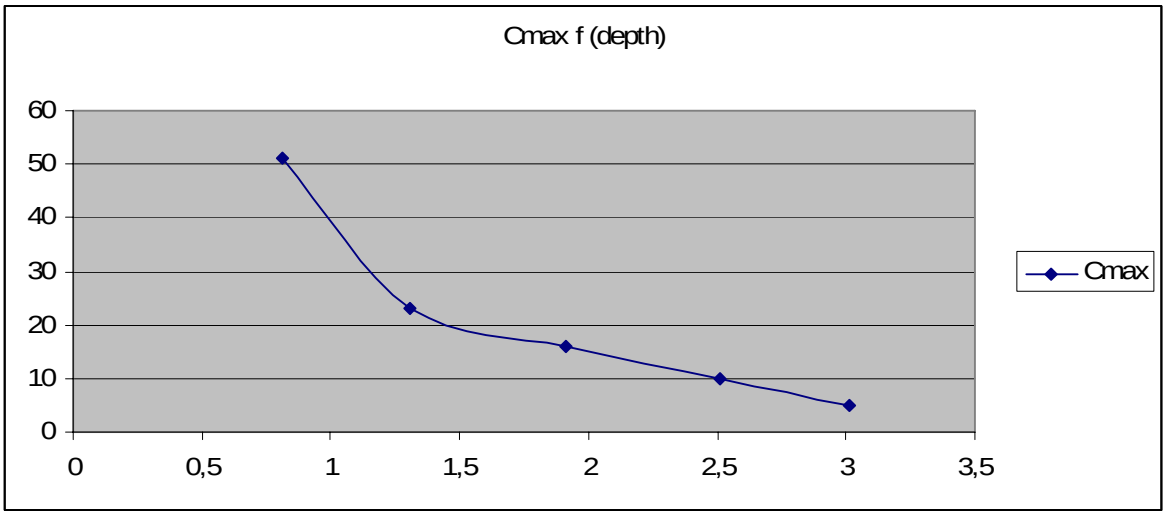

Figure 13 : Study of maximum contrast (in ADU) of defects in function of depth in mm

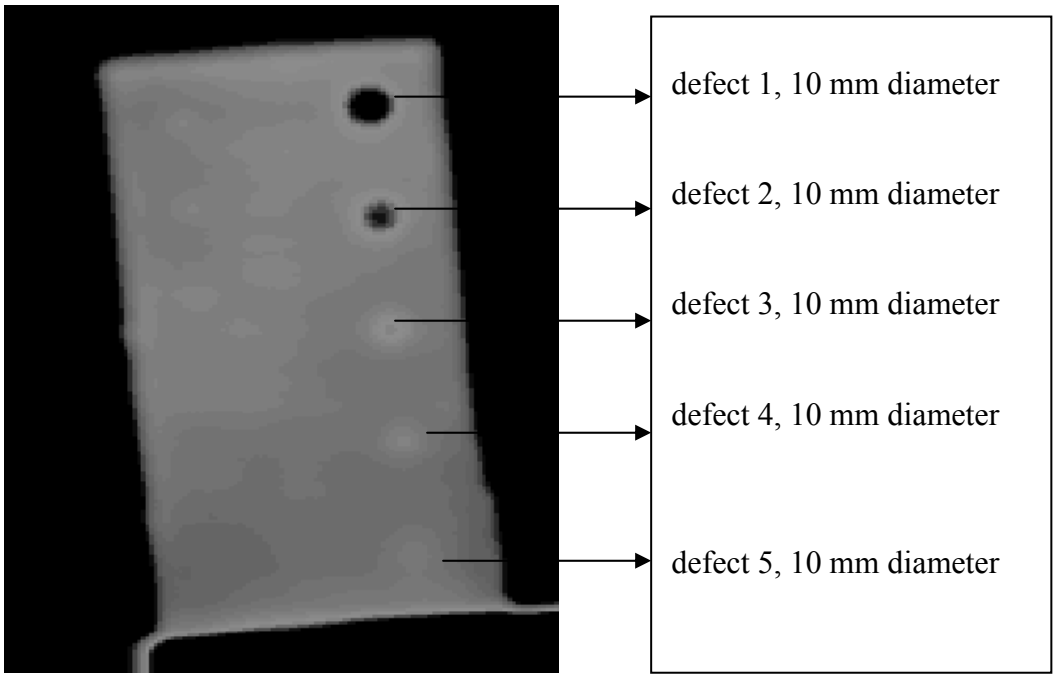

Figure 14 : CFRP panel with flat bottom holes at different depths (averaging 750 images)

By looking to figure 14, we can also see that a deep defect will appear less visible in amplitude contrast and also in size what represents for NDT community a real problem because the area of defect is a major characteristic used for acceptation or rejection of the part. The only solution is to use the information of time and amplitude of max contrast will is correlated to the depth of the defect to make post processing like DAC (Distance Amplitude Correction) in ultrasonic testing where a coefficient is applied in function of attenuation of the signal of a deep defect.

We can also distinguish 3 defects of the 5 mm row (see top left of figure 14) but we can not really take conclusions due to too the small size of these. Better quantitative analysis will be done working with temperature profile lines as seen on figure 12.

8. Numerical model of heated CFRP panel

For our simple CFRP panel (flat plate with flat bottom holes), it is here also possible to study theoretically the temperature evolution for a given heat pulse and for a given geometry of a known CFRP. The following thermal equation of Fourier has to be computed with finite elements method.

$$\frac{\partial T}{\partial t} = \frac{k}{\rho c}\left(\frac{\partial^2 T}{\partial x^2} + \frac{\partial^2 T}{\partial y^2} + \frac{\partial^2 T}{\partial z^2}\right)$$

We can here use a cylindrical model for our plate with an axial and radial heat flow with the following parameters:

Parameter	Description	Numerical Value
k axial	Axial conductivity of CFRP	0,01 $Wm^{-1}°C^{-1}$
k radial	Radial conductivity of CFRP	0,05 $Wm^{-1}°C^{-1}$
ρ	Density of CFRP	2000 kg/m³
C	Specific heat	1000 J/kg°C
Nr	Number of nodes radially	40
Na	Number of nodes axially	56
Δr	Radial step increment	1 mm
Δz	Axial step increment	0,2 mm
Frad	Radiation coefficient	$5.67e^{-12}$
Fcon	Convection coefficient	1.10^{-3} W cm^{-2}

Table 5: parameters used for our cylindrical model of heat transfer

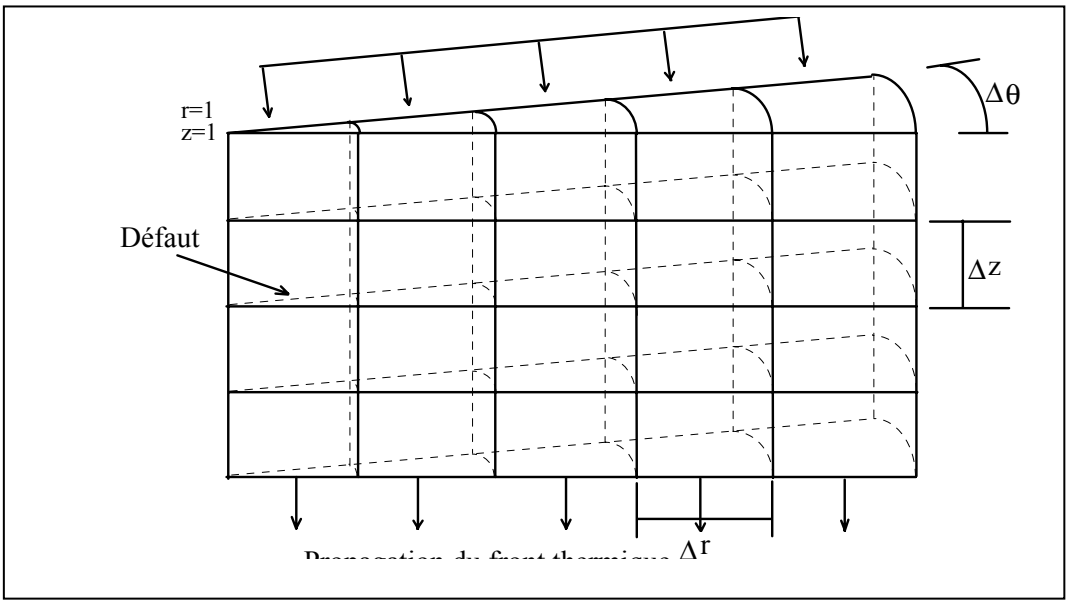

Figure 15: Description of a cake part of the cylindrical model

This simple model will easily and quickly permit us to predict the time and the visibility of any defect located at a known depth for a given heat pulse flowing axially and radially which will create a blurred and extended area of each defect in the surface temperature image as it is seen in figure 14. The following results are plotted for the computed contrast.

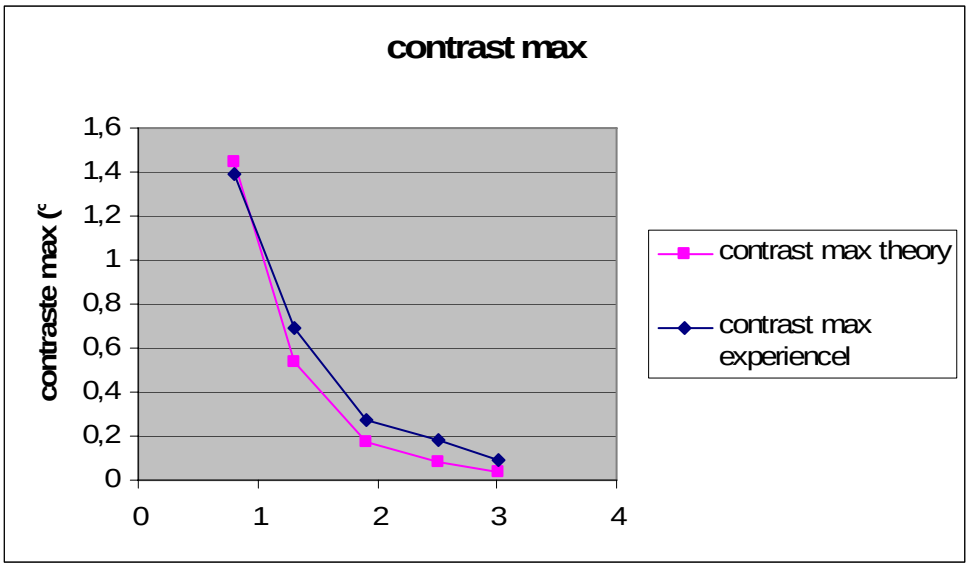

Figure 16: Evolution of max temperature contrast for the 5 defects (model and real data)

Another commercial heat transfer software (Femlab ©) was also used with a finer meshing than our rapid cylindrical model. The geometry of the plate was determined (see figure 10 left) and a finer meshing was used (see figure 17). We obtained nearly the same results for the max contrast but the computing time was 164 seconds for 19232 degrees of freedom. So we can go on with our cylindrical model for simple geometries (like circular delaminations or flat bottom holes) but not for a real composite part with honeycomb or curvature.

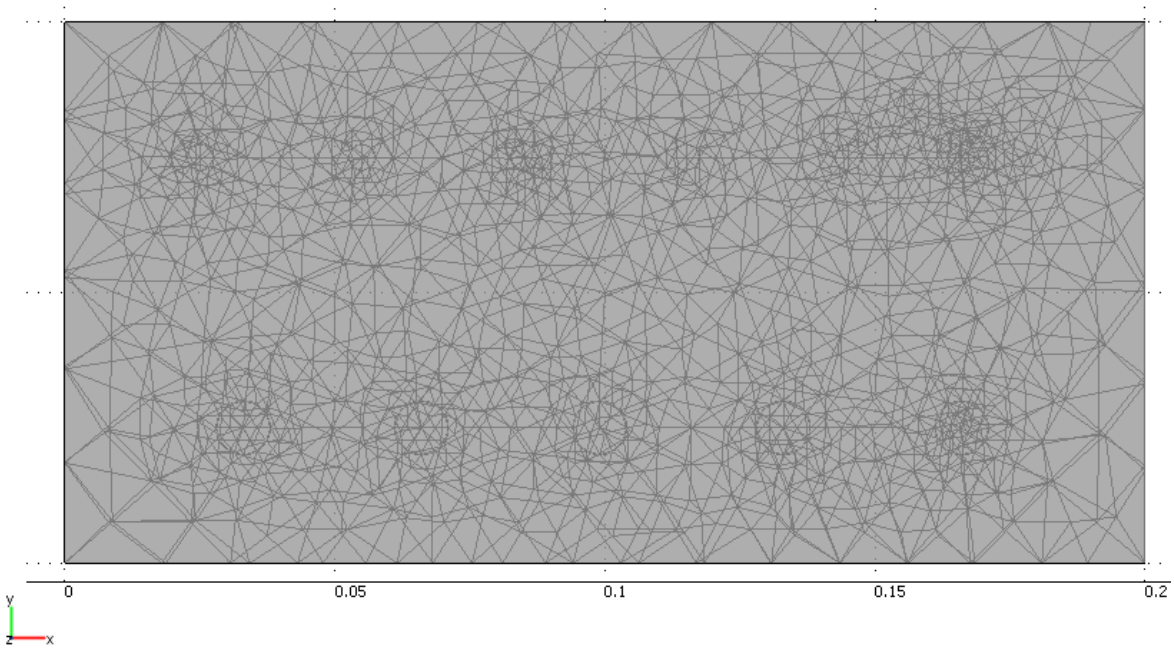

Figure 17 : Mesh of our sample with row of 5 mm defects above and five 10 mm defects below

9. Pulse Phase Thermography

Another recent technique [8] based on signal processing in frequency domain is now also possible for our thermal sequence on composite parts : Pulse phase thermography or PPT:

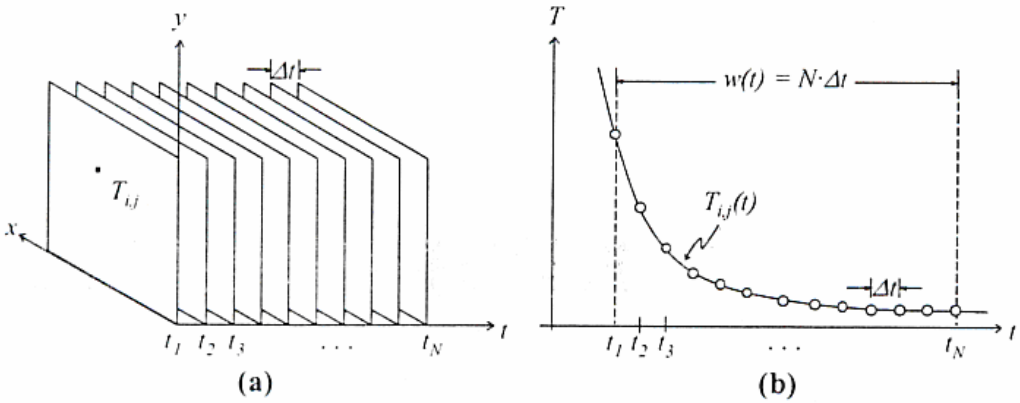

Figure 18 : (a) thermogram sequence (b) temperature evolution for one point [9]

Figure 18 (b) represents the decreasing curve for the temperature in one point after the heat pulse. This decreasing function is discrete and can be transformed in frequency domain par Fourier transformation with a well known algorithm called Fast Fourier Transform (FFT). The following equation permits to extract the different frequency components by applying the 1D Fourier transform on each pixel (i,j):

$$F_n = \sum_{k=0}^{N-1} T(k.\Delta t).e^{-i.2\pi.k.n/N} = \mathrm{Re}_n + i\,\mathrm{Im}_n$$

If we apply this transformation on each pixel for all the thermal sequence, we can also produce two types of images: amplitude and phase images. Initially modulated thermography permitted to calculate the phase shift between a thermal solicitation applied on the surface of the composite part with one frequency, using Lockin technique, thus by recording the solicitation signal and at the same time the thermal response captured by the camera.

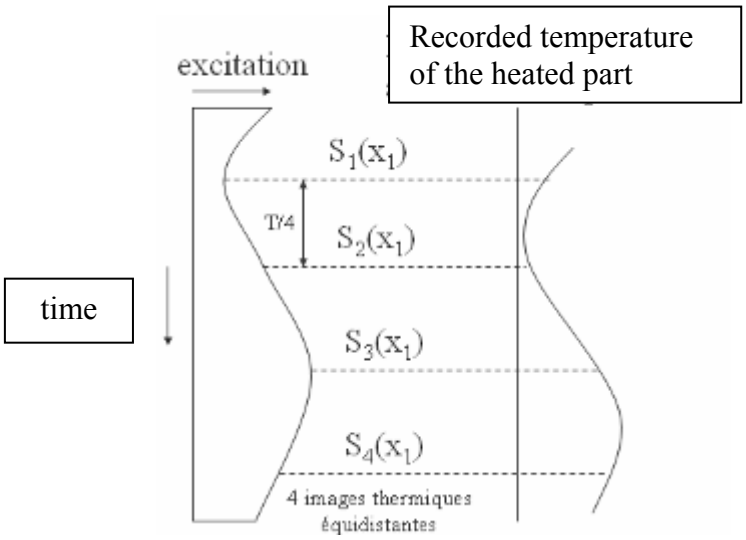

Figure 19 : Modulated thermography

To calculate the amplitude A(x1) and the phase Φ(x1) for a thermal solicitation with one frequency content, the following equation can be used:

$$\phi(x_1) = arctg\left[\frac{S_1(x_1) - S_3(x_1)}{S_2(x_1) - S_4(x_1)}\right] \qquad A(x_1) = \sqrt{[S_1(x_1) - S_3(x_1)]^2 - [S_2(x_1) - S_4(x_1)]^2}$$

By analyzing the phase equation, we see that a few problems encountered in pulse thermography can be compensated with the division of differences of images, for instance, non uniformity of heaters, variations of emissivities at entry surface (coming from variations in aerospace paintings) and secondary thermal reflections. The following figures (20 and 21) are good illustrations of this:

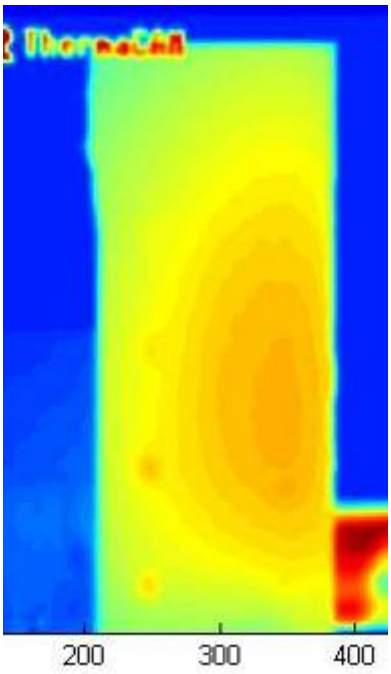

Figure 20 : non uniformity of heat in pulse thermography

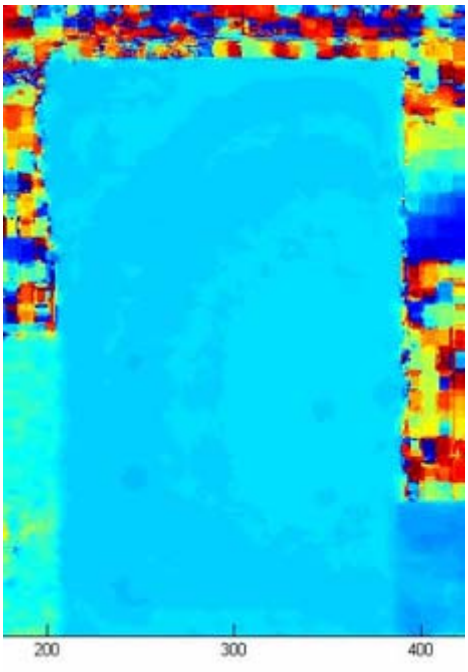

Figure 21 : phase image, low frequency in pulse phase thermography

The detection depth of defect is also an advantage when compared to classical pulse thermography. Low frequency images will show the deepest defects as it is shown in the following equation of the thermal diffusion length [9]

$\mu = \sqrt{\frac{2\alpha}{\omega}}$ with $\omega = 2\pi.f$ and α being the thermal diffusivity given by: $\alpha = \frac{k}{\rho.C_p}$

k = thermal conductivity en W/m.°C
ρ = density in kg/m³ and C_p = specific heat in J/kg.°C

The classical value of the thermal diffusivity for CFRP is $\alpha = 0.42$ m²/s.
Some authors have reported a detection depth till 2.μ [10].
We can also notice that the lower the frequency, the deeper the penetration like in Eddy Current NDT method. To have a low first frequency available in PPT, we must acquire a long time because this frequency in Hz is given by the following equation:

$$f_1 = \frac{1}{w(t)} = \frac{1}{N.\Delta t} = \frac{f_{sampling}}{N}$$

The sampling frequency is 25 Hz for our thermal imagers (PAL video signal) and the number N of images is function of the duration of the video sequence. 10 seconds will thus give N=250 images with a first frequency at 0,10 Hz and a thermal diffusion length μ = 1,2mm. If we decrease the frequency by increasing the duration of the acquisition, we can inspect deeper: for 100 seconds, we obtain now a frequency of 0,01Hz and a value of μ = 3,7 mm. The following picture will show also that higher the frequency, noisier the images:

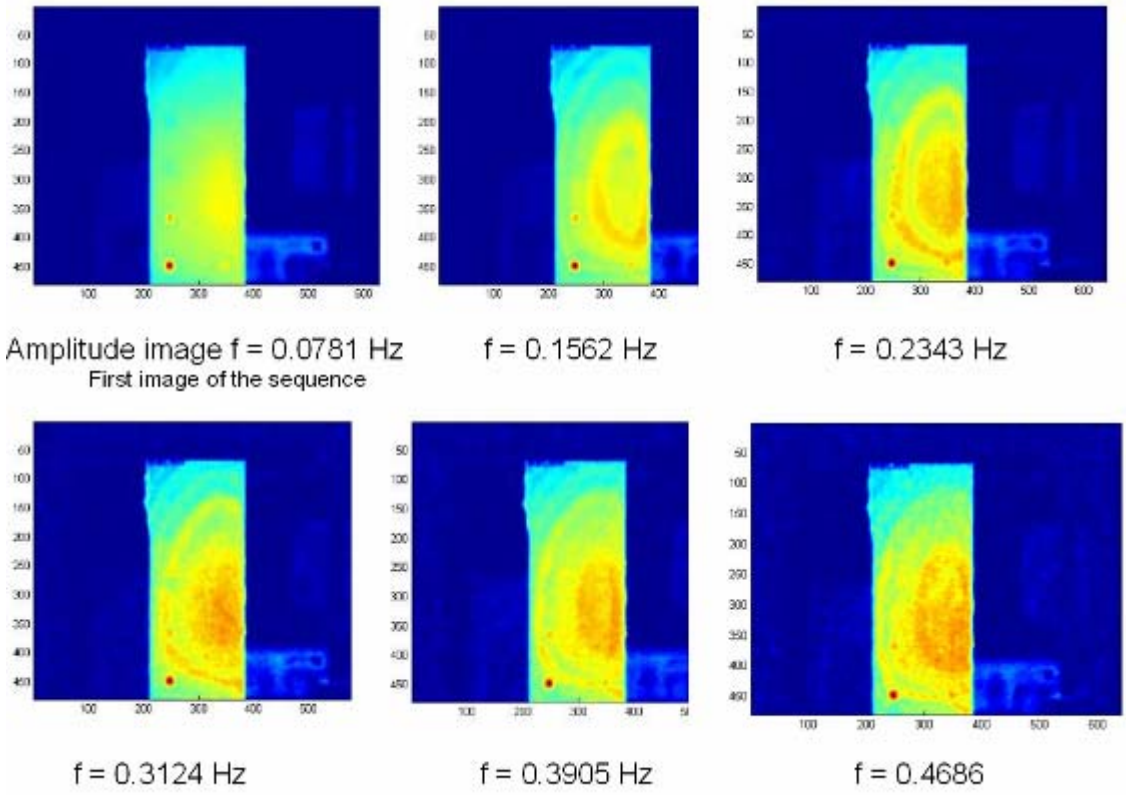

Figure 22 : 6 first amplitude images in PPT, N = 13 seconds, one halogen 500W lamp

We notice that the frequency "samples" the heat diffusion with the lowest frequency image (see top left) corresponding to a static classical thermography. A 3D view (figure 23) permits to visualize the defects of 10 and 5 mm diameters (2 first depths corresponding to one frequency image)

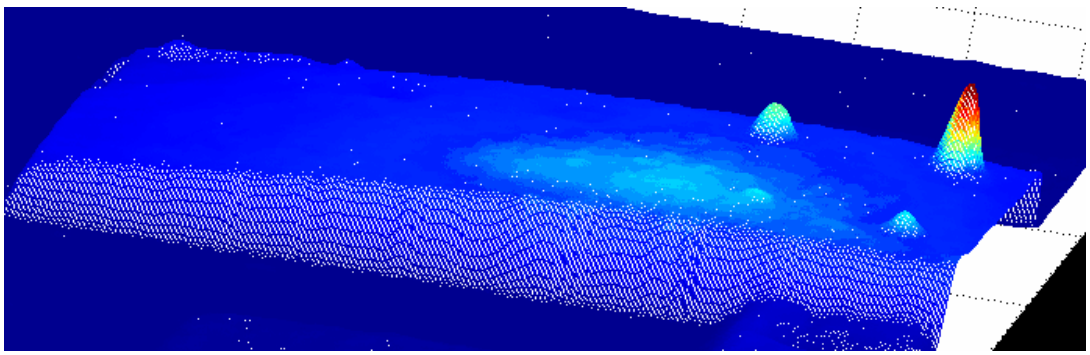

Figure 23 : 3D view of shallow defects (diameter 10 and 5 mm) - CFRP calibre

As mentioned in chapter 7, a temperature profile (figure 24) across the row of 10 mm defects will reveal the good detectability of PPT where the deepest defect located at 3 mm appears in amplitude image for a 13 seconds acquisition and a two seconds heat pulse. Pulse thermography could not detect this defect for the same setup and heat pulse duration.

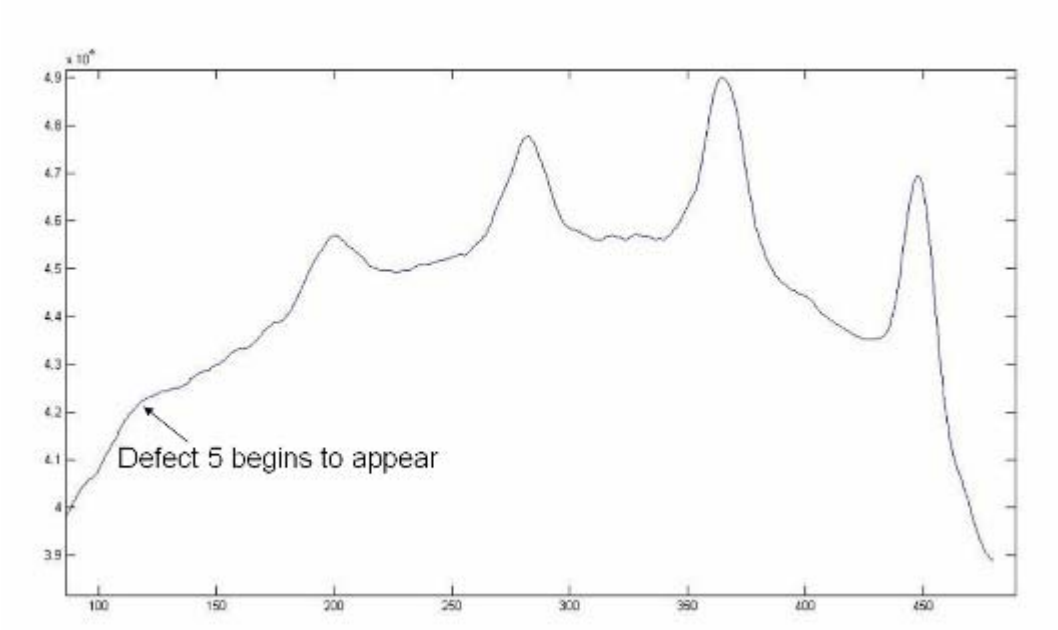

Figure 24 : Temp profile showing the deepest defects comes out of the noise in amplitude image

One other big advantage of PPT is the capability of analyzing different frequencies with one acquisition sequence when Lockin thermography asks a new thermal solicitation for each frequency. Pulse phase thermography permits us to isolate layers per layers the inspected composite piece giving thus a tomothermography like tomoscopy in radiographic testing. So low frequencies will always show the deepest defects (see figure 25) where defects 4 and 5 (or respectively layers between 2,5 and 3 mm) are emphasized.

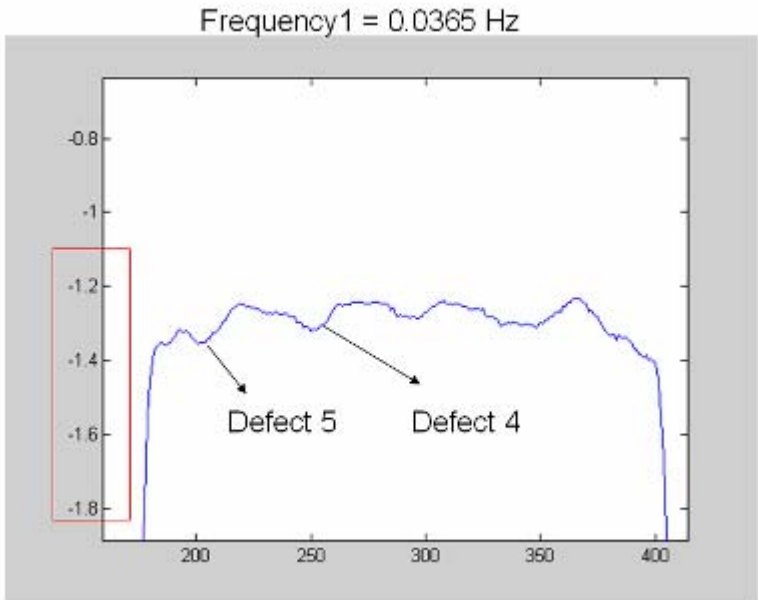

Figure 25 : temperature profile from low frequency phase image

A longer duration of heat pulse and acquisition time helps to « see » deeper in the CFRP (till more than 3 mm).

10. Conclusion

10.1 detectability

Pulse thermography is a global method which can replace radiography or ultrasonic inspection for big composite parts with skin in CFRP thinner than 3 mm. This method can detect defects bigger than 10 mm which is most of the time enough regarding the rejection criteria used in aircraft maintenance composite (classically around an half inch size). To increase the detectability, phase thermography like lockin of pulse phase thermography should be the next keeping always in mind the portability of the method.

10.2 Validation of the NDT technique

As always in NDT, a new technique must be statistically validated in the near future by use of POD (Probability Of Detection) and compared with radiography and ultrasonic C-Scan of the parts. The idea is to characterize the defect detected with 90% of POD following the methodology defined in Working Group of RTO AVT051 [6].

10.3 Application of the NDT technique to the fleet

The whole fleet of Belgian F-16 and Agusta helicopters will be inspected next year with this technique for composite parts in order to detect defects and to characterize them in accordance with the manufacturer's rejection criteria.

10.4 Edition of a NDT technique user guide, course and certification scheme

For the NDT technicians of the industry, it is also important to establish a reference training Handbook for level 1, 2 and 3 and to certify people into thermography. The used samples and the rejected flying parts are collected for training and examination at our certification centre of the Belgian National Aerospace NDT Board to be able to certify people following NAS410 or EN4179 which does not for the moment recognize thermography but probably will be the case in the near future.

References

[1] Nondestructive Testing Handbook, Third Edition, Vol 3 Infrared and Thermal Testing, Chap 15, ASNT, 2001, p495-496

[2] ASTM E 1543, Test Method for Noise Equivalent Temperature Difference of Thermal Imaging System, 1994

[3] RTO-MP-AVT-124, Water detection in Honeycomb structures by use of Thermography, RTO Publication, 2005, p28-3

[4]ASTM E 1213, Standard Test Method for Minimum Resolvable Temperature Difference for Thermal Imaging System, 1997

[5] Nondestructive Testing Handbook, Third Edition, Vol 3 Infrared and Thermal Testing, Chap 20, ASNT, 2001, p 695

[6] The Use of Field Inspection Data in the Performance Measurement of Nondestructive Inspections Final Report of the Applied Vehicle Technology Working Group 051, RTO publication

[7] Performance of FPA IR cameras and their improvement by time, space and frequency data processing. Part I: Intrinsic characterization of the thermographic system, QIRT Journal Vol. 2 No 1, P. Levesque, P. Brémond, J.L. Lasserre, A. Paupert, D.L. Balageas, 2005.

[8] Maldague X. and Marinetti S., "Pulse Phase Infrared Thermography", J. Appl. Phys., vol 79, no 5, 1996, p2694-2698.

[9] Ibarra-Castanedo C. and Maldague X., “Pulsed Phase Thermography Reviewed”, QIRT journal n°1/2004, p 47-70.
[10] Couturier J-P. and Maldague X., “Pulsed Phase Thermography of Aluminum Specimens”, Proc. SPIE, vol 3056, 1997, p. 170-175.